J Solid State Electrochem (2011) 15:1071–1075
DOI 10.1007/s10008-010-1288-1

ORIGINAL PAPER

Oxygen non-stoichiometry, high-temperature properties, and phase diagram of $CaMnO_{3-\delta}$

Ekaterina I. Leonidova · Ilya A. Leonidov · Mikhail V. Patrakeev · Victor L. Kozhevnikov

Received: 26 November 2010 / Revised: 23 December 2010 / Accepted: 29 December 2010 / Published online: 12 February 2011

Abstract The oxygen content in $CaMnO_{3-\delta}$ is studied by a coulometric titration technique depending on temperature and oxygen partial pressure variations in the ambient atmosphere. The δ–T phase diagram is derived from the obtained data where single-phase fields are outlined for orthorhombic, tetragonal, and cubic structures. The thermal expansion coefficient considerably larger in the cubic phase than in the tetragonal one is related with formation of large Mn^{3+} cations at depletion of oxygen from the crystalline lattice. Negative thermopower is explained by concomitant reactions of oxygen loss and charge disproportionation, $2Mn^{4+} = Mn^{3+} + Mn^{5+}$. The forbidden energy gap in $CaMnO_{3-\delta}$ is evaluated to be about 0.5 eV.

Keywords Calcium manganite · Perovskite · Oxygen non-stoichiometry · Phase diagram · Electrical properties · Charge disproportionation · Thermal expansion

Introduction

Perovskite-like manganites $La_{1-x}A_xMnO_{3-\delta}$, where A is typically Ca, Sr or their mixture, exhibit a number of unusual and practically important electric and magnetic properties that are intimately related with electronic configuration of manganese cations and structural peculiarities of the crystalline lattice [1–4]. The high electrical conductivity and catalytic activity of manganites make them attractive candidate materials for applications in solid oxide fuel cells and for electrochemical removal of NO_x [5, 6]. The changes in the oxidation state of manganese can be achieved by dissolution of $CaMnO_{3-\delta}$ or $SrMnO_{3-\delta}$ in the matrix manganite $LaMnO_{3+\delta}$ and by heat treatments at different pressures of oxygen [7, 8]. Since doping and heating are both accompanied with structural transitions, phase diagrams for manganite systems are the subject of intense research. Most detailed data concerning x–T diagrams are obtained for $La_{1-x}A_xMnO_{3-\delta}$ and $Ca_{1-x}Sr_xMnO_{3-\delta}$ at low temperatures where oxygen content remains invariable [9–13]. On the other hand, less studied in manganites are interrelations of structural types and phase stability borders at high-temperature variations of oxygen content, i.e., δ–T diagrams. Thus, the influence of oxygen content upon high-temperature phase transitions is reviewed in $LaMnO_{3+\delta}$ [8]. More recently phase transformations in the system $SrMnO_{2.5}$–$SrMnO_{3.0}$ were studied depending on temperature and oxygen content. The temperature stability limits were established for $Sr_2Mn_2O_5$ (δ=0.5), $Sr_5Mn_5O_{13}$ (δ=0.4), and $Sr_7Mn_7O_{19+\delta}$ (δ~0.3) [14]. These phases are members of the new homologous series $Sr_{4+m}Mn_4{}^{3+}Mn^{4+}{}_mO_{10+3m}$ of oxygen vacancy-ordered perovskite manganites built from $Mn^{3+}O_5$ pyramids and $Mn^{4+}O_6$ octahedra, and they are stable in heavily reducing conditions [15, 16]. According to [15], structurally similar homologs are calcium manganites $CaMnO_{2.5}$ [17], $CaMnO_{2.667}$ [18], и $CaMnO_{2.75}$ [19], which can be obtained in hydrogen containing atmosphere at 300 °C. However, information about the phase diagram for $CaMnO_{3-\delta}$ is rather scarce.

Stoichiometric $CaMnO_3$ has an orthorhombic structure at room temperature [17]. The high-temperature X-ray diffraction and differential thermal analysis show that when heated in air, this phase drops off oxygen and transforms

E. I. Leonidova (✉) · I. A. Leonidov · M. V. Patrakeev · V. L. Kozhevnikov
Institute of Solid State Chemistry, Ural Branch of Russian Academy of Sciences,
91 Pervomaiskaya Str.,
Ekaterinburg, Russian Federation
e-mail: katrine@ihim.uran.ru

into a tetragonal modification at 896 °C and then in a cubic phase at 913 °C [20]. The same sequence of phase transitions in $Ca_{1-x}Sr_xMnO_{3-\delta}$ is confirmed by in situ high-temperature neutron diffraction complemented with detailed consideration of changes with temperature of bond lengths (Ca,Sr)–O and Mn–O and of tolerance factors [11, 21]. The variations of oxygen content in $CaMnO_{3-\delta}$ at heating are measured at $3\cdot10^{-6}$, 0.21 and 1 atm [8]. High-temperature studies [22] at low oxygen pressures evidence decomposition of non-stoichiometric $CaMnO_{3-\delta}$ into mixture of Ca_2MnO_4 and $CaMn_2O_4$.

The aim of this work is to determine δ–T phase boundaries for polymorphic modifications and to study effects of high-temperature phase transitions upon electric properties and thermal expansion in $CaMnO_{3-\delta}$.

Experimental

High purity calcium carbonate $CaCO_3$ and manganese oxide Mn_2O_3 were used for the synthesis of $CaMnO_{3-\delta}$. The starting reagents taken in desirable amounts were placed in a quartz glass where nitric acid was then added till their complete dissolution. After this, the amino-acetic acid was added to form a homogeneous gel. The gradual heating of the gel resulted in desiccation followed by ignition and burning of the gel. The obtained fine black powder was pressed under uni-axial pressure into pellets of 2 mm thickness and 12 mm diameter. The pellets were fired in air at 900 °C during 2 h. Then temperature was raised to 1320 °C where calcination continued for 10 h, after which the samples were cooled down to room temperature with the rate of 1 °C/min. The apparent density of the samples was about 95% of theoretical.

The obtained specimens were analyzed by X-ray powder diffraction at room temperature using a Shimadzu XRD-7000 diffractometer equipped with CuK_α-radiation. Finely ground sample powder was scanned within $10<2\Theta<90°$. The diffraction patterns were refined to confirm single phase samples of the orthorhombic perovskite-like calcium manganite with the elementary unit parameters a=5.281(1), b=7.453(1), and c=5.266(1) Å.

Thermal analysis was carried out in air and in 5% O_2:95%Ar gas mixtures with the help of a Setaram Setsys Evolution apparatus. Thermal expansion up to 1000 °C in air was measured with the using of a Linseis L75 dilatometer. The heating rate was 10 °C/min.

The oxygen content variations with respect to a reference point were measured as a function of oxygen partial pressure and temperature by means of the coulometric titration technique in the double electrochemical cell, as described elsewhere [23]. The uncertainty of the measurements is $\Delta\delta=\pm0.001$. The oxygen content (3-δ) for $CaMnO_{3-\delta}$ was determined by thermogravimetric analysis (TGA). The initial value (3-δ)=3.0 for oxygen content agrees with data [8, 21].

Sintered pellets were cut into bars for electric conductivity and thermopower characterization at heating in air. The sample for thermopower measurements was placed along natural temperature gradient in the furnace (about 15 °C/cm). Two S-type thermocouples were attached to the butt ends of the sample after sheets of Pt foil; the Pt leads of the thermocouples served also as thermovoltage probes. The measured results were corrected for the contribution of platinum [24]. For the conductivity measurements by the four-probe d.c. technique, the second sample was placed in a crosswise orientation near the middle of the sample for thermopower measurements, i.e., in an isothermal plane. The electrical parameters of the experiment were measured using a high-precise voltmeter Solartron 7081.

Results and discussion

The obtained Po_2–T–δ diagram for $CaMnO_{3-\delta}$, i.e., the oxygen content variations with oxygen partial pressure at different temperatures, is shown in Fig. 1. One can see three-phase regions with different slopes of the (3–δ) vs. $\log p_{O_2}$ isotherms. The oxygen content in the orthorhombic phase depends only weakly on oxygen pressure while substantially larger derivatives $\partial(3-\delta)/\partial\log p_{O_2}$ are characteristic for the tetragonal modification. The slope for the isotherms in the cubic phase is somewhat smaller than in the tetragonal phase, and it tends to increase with the pressure decrease. The phase borders for different crystalline modifications of $CaMnO_{3-\delta}$ are shown in the Po_2–T–δ diagram with dashed lines. The temperature increase results in enlargement of the existence domain for the cubic phase

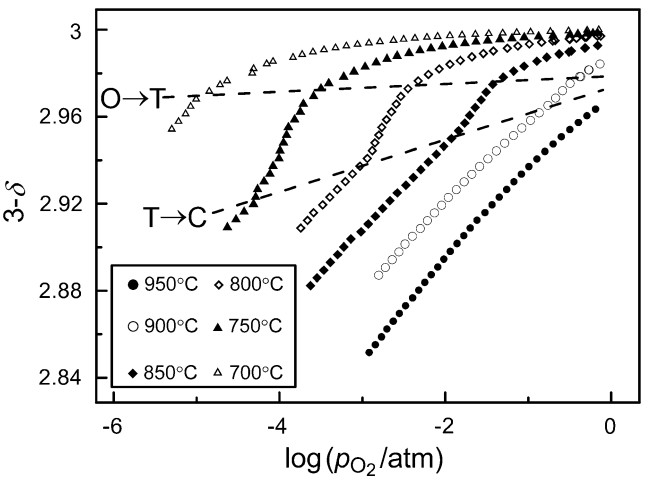

Fig. 1 Oxygen content changes in $CaMnO_{3-\delta}$ vs. oxygen partial pressure at different temperatures

while the respective field for the tetragonal phase becomes smaller. The isotherms $(3-\delta)-\log p_{O_2}$ obtained at 850 and 950 °C in the course of the present study are shown in Fig. 2 together with the isotherm at 1000 °C from [22]. It may be noticed that the thermodynamic stability borders at different temperatures are marked with oxygen content changes in the specimen at permanent values of oxygen pressure. Following [22] one can conclude that these Po_2's correspond to the equilibrium of the gas phase oxygen with the mixture of the parent cubic manganite $CaMnO_{3-\delta}$ and its decomposition products, Ca_2MnO_4 and $CaMn_2O_4$. The low-pressure stability border for the cubic phase is shown with dashed line in Fig. 2. It is seen that decomposition of $CaMnO_{3-\delta}$ at 850 °C occurs when δ approaches 0.18 while it does not exceed 0.2 at 1000 °C. The limiting values for δ and Po_2 are in excellent agreement with the results [22].

The δ–T diagram in Fig. 3 is derived from Fig. 1. It is seen clearly that the existence range for the cubic phase is rapidly narrowing with the temperature decrease. One can conclude that the non-stoichiometric $CaMnO_{3-\delta}$ with the cubic structure under normal conditions can be obtained only by quenching after equilibration above 600 °C at low pressures of oxygen. The phase transition from the orthorhombic to tetragonal modification (O↔T) occurs within a narrow δ range, $0.02<\delta<0.04$, which agrees with [8] where it is shown that in air it takes place when $\delta=0.025$. The transition temperature tends to sharply decrease even with a slight increase in δ as it can be seen also from comparison of DTA curves obtained in air and in the 5% O_2:95%Ar gas mixture, Fig. 4.

The measurements in air demonstrate strong influence of oxygen content and phase transitions upon thermal expansion of $CaMnO_{3-\delta}$, Fig. 5. The relative linear expansion in the orthorhombic phase ($\Delta L/L_0$) increases nearly linearly with temperature, which results in only weak variations of the thermal expansion coefficient $\alpha=(dL/dT)/L_0$ within

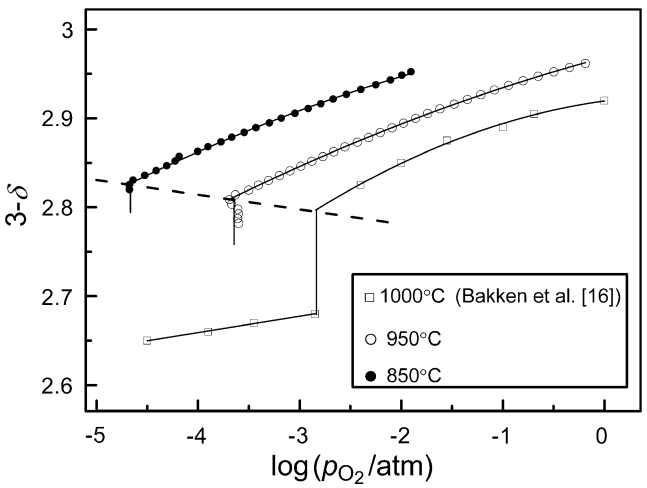

Fig. 2 Oxygen content in $CaMnO_{3-\delta}$ at low pressures of oxygen

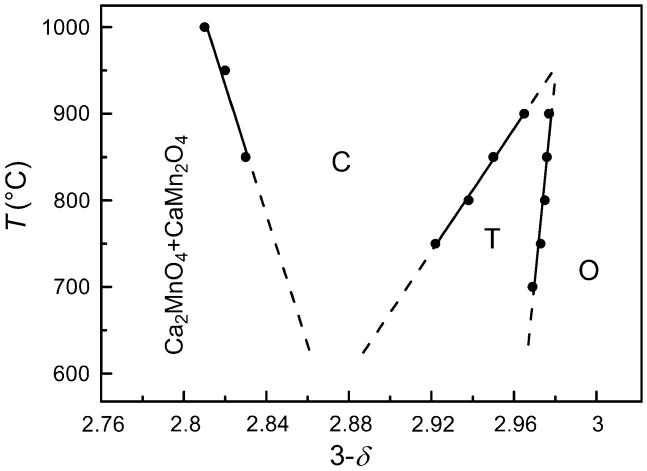

Fig. 3 Phase diagram for $CaMnO_{3-\delta}$. The cubic, tetragonal and orthorhombic structural modifications are designated as C, T, and O, respectively

120–600 °C, where oxygen exchange is suppressed. At the same time, the loss of oxygen at further heating and transition to the tetragonal phase near 900 °C results in a fast increase of the thermal expansion coefficient to about $35\cdot10^{-6}$ K^{-1}. The thermal expansion coefficient achieves nearly $30\cdot10^{-6}$ K^{-1} in the cubic phase where it also does not exhibit any appreciable dependence on temperature. The increase of the thermal expansion coefficient at heating and oxygen loss above 600 °C is related with the formation of Mn^{3+} cations with the size larger than of Mn^{4+} cations [25].

The measured data on electric conductivity and thermopower in $CaMnO_{3-\delta}$ are shown in Fig. 6. One can see rather small temperature activated conductivity that is typical for electron transport via jumps of small polarons in the entire measured range 300–950 °C [26]. The obtained values differ somewhat from [27]. The discrepancy can be attributed to the difference in extended defects such as grain boundaries. Unlike electric conductivity, the thermoelectric power is not strongly influenced by a polycrystal-

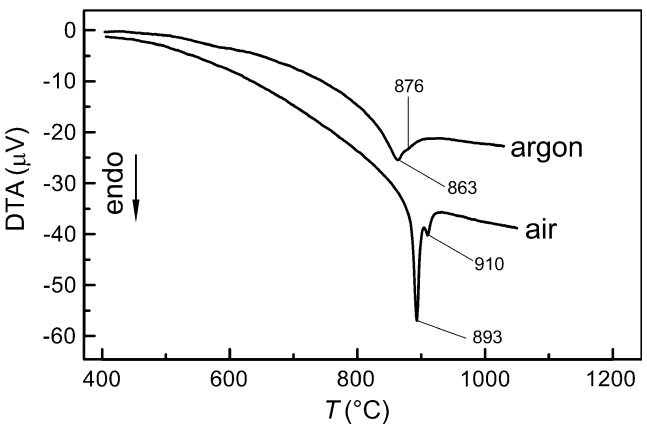

Fig. 4 DTA curves for $CaMnO_{3-\delta}$ at heating in air and 95%Ar:5%O_2 gas mixture

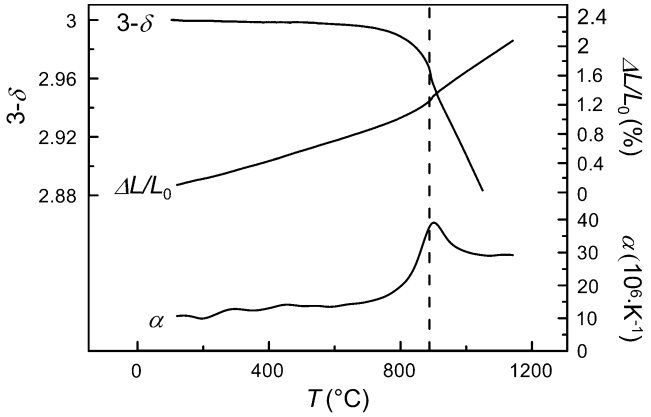

Fig. 5 Variations of oxygen content, relative elongation, and thermal expansion coefficient with temperature at heating of $CaMnO_{3-\delta}$ in air

line character of the specimens, which enables a meaningful comparison of the data from different authors. Thus, the thermopower values obtained in this work at room temperature are corroborated by the results [28, 29]. The absolute values of thermopower increase with heating nearly linearly from 320 μV/K at room temperature to 350 μV/K at ~200 °C. Measurements below room temperature show also that this behavior can be observed from antiferro- to paramagnetic state transition near 130 K [29, 30]. According to [29] the metallic-like thermopower in $CaMnO_{3-\delta}$ reflects small binding energy of polaronic carriers in electron-doped calcium manganite, when initial and final states are separated in energy by less than kT. Neglecting this weak temperature dependence one can employ the Heikes [31] expression

$$S = -\frac{k}{|e|}\ln\left(\frac{1-n}{n}\right), \quad (1)$$

in order to evaluate the concentration, n~0.02, of electrons, i.e., Mn^{3+} cations, that result in appearance of the

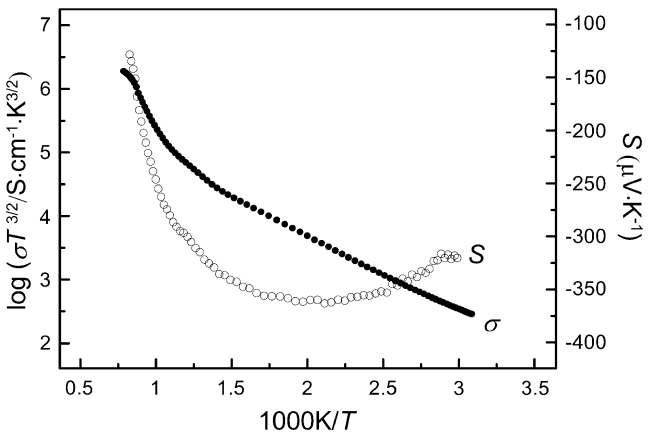

Fig. 6 Variations of conductivity and thermopower vs. inverse temperature at heating of $CaMnO_{3-\delta}$ in air

thermovoltage of about 300–350 μV/K in $CaMnO_{3-\delta}$. Since $n=2\delta$ one can see that oxygen deficiency in the as prepared samples is near δ~0.01. This small value agrees with works [8, 21] where it is shown that nearly stoichiometric calcium manganite can be obtained at high-temperature annealing followed by slow cooling in air.

The thermopower shows transition to semiconductor-like behavior at heating above ~200 °C. This change was described earlier in [27] where it was claimed to be a manifestation of a metal to insulator transition. However, it is not accompanied with any appreciable variations in conductivity. Moreover, it can be observed that the concentration of electrons (Mn^{3+} cations) as calculated with (1) occurs systematically larger at elevated temperatures than it follows from the non-stoichiometry data in Fig. 1. Therefore, one can suggest that besides of the oxygen depletion

$$2Mn^{4+} + O^{2-} = 2Mn^{3+} + V_O + \frac{1}{2}O_2 \quad (2)$$

one more thermally activated reaction, viz., charge disproportionation

$$2Mn^{4+} = Mn^{3+} + Mn^{5+} \quad (3)$$

takes place also, which favors the concentration increase of electrons. Reaction 3 is directly evidenced by the thermopower changes, Fig. 6, in the temperature range 220–550 °C where oxygen non-stoichiometry δ is invariable according to thermal analysis. The increase in concentration of Mn^{3+} cations results in respective decrease of the ratio $(1-n)/n$ in Eq. 1 and, therefore, in decrease of absolute values of thermopower $|\alpha|$ with the temperature increase.

The holes can be considered as immobile because hole jumps over t_{2g} states of Mn^{5+} and Mn^{4+} cations seem to be rarely observed relative to the more frequent electron jumps over e_g states of Mn^{3+} and Mn^{4+} cations. As disproportionation is a transfer of electrons from the half-filled t_{2g} band to the empty e_g band of Mn^{4+} cations [4], the enthalpy ΔH for reaction 3 is to be about the width of the forbidden gap E_g in the manganite. From the slope of the $\log(\sigma T^{\frac{3}{2}})$ vs. $1/T$ plot [26] one can obtain E_g~0.5 eV, which is in a reasonable correspondence with the calculated value 0.7 eV in [32].

The appearance of rather large Mn^{3+} ions results in the increase of the average size of manganese cations and promotes the O↔T phase transition. The phase diagram demonstrates a sharp decrease of the existence range of the tetragonal phase at heating so that direct transition from the orthorhombic to cubic structure may occur above 1000 °C. The transition can be explained as a consequence of the charge disproportionation, which results in the appearence of $Mn^{3+}O_6$ и $Mn^{5+}O_6$ octahedra with greatly differrent volumes [25]. The multiple presence of such octahedra in

the structure of $CaMnO_{3-\delta}$ leads to deviation of the bond angles Mn-O1-Mn and Mn-O2-Mn from the values near 160° that are necessary for formation of the orthorhombic structure [11, 17], and the manganite aquires cubic structure.

Conclusion

The oxygen content variations at different temperatures and pressures of oxygen are studied in $CaMnO_{3-\delta}$ by means of the coulometric titration technique. The data are used in order to obtain the phase diagram where stability fields of orthorhombic, tetragonal and cubic structures are shown depending on oxygen content and temperature. It is shown that the orthorhombic phase is stable at 700–950 °C when $\delta <$ 0.04. The phase transition from the orthorhombic to tetragonal structure occurs in the narrow range $0.02 < \delta <$ 0.04. The thermal expansion coefficient is shown to increase at the transition. The temperature increase results in considerable enlargement of the homogeneous range of oxygen content in the cubic structure. Both negative thermopower and temperature activated conductivity are explained as a consequence of the oxygen loss and charge disproportionation reactions. The forbidden band gap in $CaMnO_{3-\delta}$, which corresponds to the energy difference between the half-filled t_{2g} and empty e_g bands of Mn^{4+} ions, is evaluated to be about 0.5 eV.

Acknowledgments The authors are thankful to RF Samigullina and AA Markov for the help in TGA and conductivity measurements. Support of this work by the Russian Foundation for Basic Research under grant №10-03-00475a is gratefully acknowledged.

References

1. Jin S, Tieffel TH, McCormack M, Fastnacht RA, Ramesh R, Chen LH (1994) Science 264:413–415
2. Ju HL, Kwon C, Li Q, Greene RL, Venkatesan T (1994) Appl Phys Lett 65:2108–2110
3. Dabrowski B, Dybzinski R, Bukowski Z, Chmaissem O, Jorgensen JD (1999) J Solid State Chem 146:448–457
4. Mukhin AA, Ivanov VY, Travkin VD, Lebedev SP, Pimenov A, Loidl A, Balbashov AM (1998) JETP Lett 68:356–362
5. Radhakrisnan R, Virkar AV, Singhal SC (2005) J Electrochem Soc 152:A210–A218
6. Werchmeister RML, Hansen KK, Mogensen M (2010) Mater Res Bull 45:1554–1561
7. Mizusaki J, Mori N, Takai H, Yonemura Y, Minamiue H, Tagava H, Dokiya M, Inaba H, Naraya K, Sasamoto T, Hashimoto T (2000) Solid State Ionics 129:163–177
8. Rørmark L, Wiik K, Stølen S, Grande TJ (2002) Mater Chem 12:1058–1067
9. Schiffer P, Ramirez AP, Bao W, Cheong S (1995) Phys Rev Lett 75:3336–3339
10. Hemberger J, Krimmel A, Kurz T, von Krug Nidda HA, Ivanov VY, Mukhin AA, Balbashov AM, Loidl A (2002) Phys Rev B 66:094410
11. Chmaissem O, Dabrowski B, Kolesnik S, Mais J, Brown DE, Kruk R, Prior P, Pyles B, Jorgensen JD (2001) Phys Rev B 64:134412
12. Dunaevskii SM (2004) Phys Solid State 46:193–212
13. De Renzi R, Allodi G, Amoretti G, Guidi MC, Fanesi S, Guidi G, Licci F, Caneiro A, Prado F, Sanchez R, Oseroff S, Amato A (2000) Phys B 289:85–88
14. Suescun L, Dabrowski B, Mais J, Remsen S, Richardson JW, Maxey ER, Jorgensen JD (2008) Chem Mater 20:1636–1645
15. Suescun L, Dabrowski B (2008) Acta Crystallogr B64:177–186
16. Suescun L, Chmaissem O, Mais J, Dabrowski B, Jorgensen JD (2007) J Solid State Chem 180:1698–1707
17. Poeppelmeier KR, Leonowicz ME, Scanlon JC, Longo JM, Yelon WB (1982) J Solid State Chem 45:71–79
18. Reller A, Thomas JM, Jefferson DA, Uppal MK (1984) Proc R Soc Lond A 394:223–241
19. Chiang CCK, Poeppelmeier KR (1991) Mater Lett 12:102–108
20. Taguchi H, Nagao M, Sato T, Shimada M (1989) J Solid State Chem 78:312–315
21. Dabrowski B, Chmaissem O, Mais J, Kolesnik S, Jorgensen JD, Short S (2003) J Solid State Chem 170:154–164
22. Bakken E, Norby T, Stølen S (2005) Solid State Ionics 176:217–223
23. Mitberg EB, Patrakeev MV, Lakhtin AA, Leonidov IA, Kozhevnikov VL, Poeppelmeier KR (1998) Solid State Ionics 120:239–249
24. Cusak N, Kendall P (1958) Proc Phys Soc 72:898
25. Shannon RD (1976) Acta Crystallogr A32:751–767
26. Raffaelle R, Anderson HU, Sparlin DM, Parris PE (1991) Phys Rev B 43:7991–7999
27. Thao PX, Tsuji T, Hashida M, Yamamura Y (2003) J Ceram Soc Jpn 11:544–547
28. Taguchi H, Sanoda M, Nagao M (1998) J Solid State Chem 137:82–86
29. Hejtmánek J, Jirák Z, Maryško M, Martin C, Maignan A, Harvieu M, Raveau B (1999) Phys Rev B 60:14057–14065
30. Fisher B, Patlagan L, Reisner GM, Knizhnik A (2000) Phys Rev B 61:470–475
31. Heikes RR (1961) Thermoelectricity. Wiley-Interscience, New York
32. Søndenå R, Stølen S, Ravindran P, Grande T, Grande NL (2007) Phys Rev B 75:184105